Fuel xxx (xxxx) xxxx

Contents lists available at ScienceDirect

Fuel

journal homepage: www.elsevier.com/locate/fuel

Full Length Article

Self-sustained combustion of CO with transient changes and reaction mechanism over $CuCe_{0.75}Zr_{0.25}O_{\delta}$ powder for honeycomb ceramic catalyst

Running Kang[a,b], Xiaolin Wei[a,b,c], Pandong Ma[a,d], Feng Bin[a,c,*], Junyao He[a,e], Qinglan Hao[d], Baojuan Dou[d,*]

[a] State Key Laboratory of High-Temperature Gas Dynamics, Institute of Mechanics, Chinese Academy of Sciences, Beijing 100190, PR China
[b] School of Engineering Science, University of Chinese Academy of Sciences, 100049 Beijing, PR China
[c] Dalian National Laboratory for Clean Energy, Dalian 116023, China
[d] College of Marine & Environmental Science, Tianjin University of Science & Technology, Tianjin 300457, PR China
[e] School of Energy and Power Engineering, Xi'an Jiaotong University, Xi'an 710049, PR China

GRAPHICAL ABSTRACT

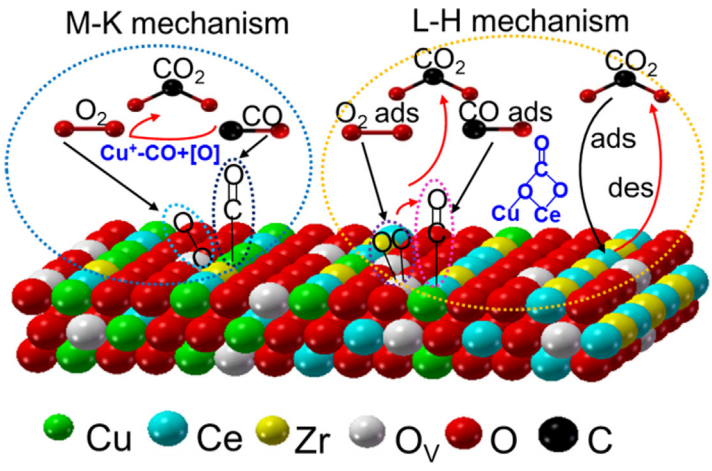

ARTICLE INFO

Keywords:
$CuCe_{0.75}Zr_{0.25}O_{\delta}$ honeycomb catalyst
Carbon monoxide
Self-sustained combustion
Reactant concentration
Transient changes
Competitive adsorption

ABSTRACT

A $CuCe_{0.75}Zr_{0.25}O_{\delta}$ catalyst was prepared by the sol-gel method and successfully coated on honeycomb ceramic (HC) carrier. The activity of $CuCe_{0.75}Zr_{0.25}O_{\delta}$/HC was determined by the CO-TPO + FLIR, with the results performing that the critical condition for CO self-sustained combustion is 3 vol% CO + 3 vol% O_2/N_2 at 0.5 L/min. As the CO concentration increases from 1 vol% CO to 3 vol% CO, the induction process ($< T_{15}$) shifts toward a slower CO conversion, while the light-off process ($> T_{15}$) shifts to rapid ignition with a transient change for the CO oxidation reaction. The furnace temperature for CO self-sustained combustion decreases with increasing the CO and O_2 concentrations. Upon increasing the CO_2 concentration, however, furnace temperature is needed to increase and realize CO complete conversion. The thermal stability test combined with SEM + EDX results indicate that the $CuCe_{0.75}Zr_{0.25}O_{\delta}$ /HC retains an excellent thermal stability after a 200 h, and the high-temperature region remains at 225 ± 1 °C during the CO self-combustion reaction. The activity of catalyst is reduced slightly after the 200 h test because of the carbon deposition on the catalyst surface, but such a slight

* Corresponding authors at: State Key Laboratory of High-Temperature Gas Dynamics, Institute of Mechanics, Chinese Academy of Sciences, Beijing 100190, PR China (F. Bin).
E-mail addresses: binfeng@imech.ac.cn (F. Bin), bjdou@tust.edu.cn (B. Dou).

https://doi.org/10.1016/j.fuel.2019.116637
Received 2 September 2019; Received in revised form 8 November 2019; Accepted 11 November 2019

deactivation can be eliminated by the air oxidation method. In situ IR results show a competitive adsorption of CO/O_2 and CO_2 on the Cu-Ce active sites, indicating that the addition of gaseous CO_2 performs an inhibition of CO oxidation. CO preferentially adsorbs linearly at Cu^+ sites to form carbonyls that react with lattice oxygen to produce CO_2 to release, which can be ascribed to M-K mechanism. The L-H mechanism is less important, which involves the relatively weak reaction of adsorbed CO and adsorbed oxygen on the Cu-Ce active sites to form carbonate species.

1. Introduction

The off-gas produced from steelmaking usually contains approximately 40–70 vol% of carbon monoxide (CO), which is important to recycle and use as a fuel [1]. However, the concentration of CO decreases to 20 vol% at the beginning and end of steelmaking intermissions. Due to the possibility of CO and O_2 mixture causing explosions, these off-gases that are present during steelmaking intermissions are often discharged into the atmosphere by methane combustion-supporting flare burners rather than being recovered directly [2], which results in a substantial waste of energy and environmental pollution via the direct methane combustion strategy.

Catalytic self-sustained combustion can be accepted as an economical and effective strategy for off-gas combustion without heat input. Considering the concentration fluctuation of off-gas (0–15 vol% CO, 3–15 vol% O_2 and 10–40 vol% CO_2) during the tap-to-tap cycle, the challenges of this technology, which are related to the ignition process, limit of self-sustaining combustion and durability, etc., are to design an effective industrial catalyst that provides stable operation for an extended period of time. In recent decades, mixed metal oxide powder catalysts, including Cu, Ce and Zr, have been studied widely during low-temperature CO oxidation due to their high activity, good sintering resistance and low cost [3–5].

Many reports have focused on the structure-activity relationships and transient changes in the ignition of CO oxidation over Cu-Ce-Zr powder catalysts [6–8]. With respect to the important structure-activity relations for CO catalytic combustion, Jia et al. found that the CuO species on the surface and Cu-Ce solid solution involve the oxidation of CO, where the former provides a high activity site for CO chemisorption and the latter promotes a large number of oxygen vacancies [9]. In our previous research, the reaction sensitivity and activity of different active sites were determined to have the following order: surface CuO_x > Cu-Ce-O_δ solid solution > Ce-Zr-O_δ solid solution over a powdered $CuCe_{0.75}Zr_{0.25}O_\delta$ catalyst [10].

The catalytic ignition process with a variation in the reactant concentration is also an unavoidable step of CO catalytic combustion on active sites. It is crucial to understand catalytic surface reactions for process safety and the initiation of complete combustion systems. Upon considering transient changes in the ignition process for CO catalytic combustion, Skoglundh et al. observed a transient shift during the start conversion of CO by quickly switching different gas compositions [11]. Carlsson et al. also suggested that pulsing O_2 led to an increased CO conversion rate transient because the O_2 addition reduced the self-poisoning by CO, hence promoting the reaction rate for CO oxidation [12]. Recently, our previous work confirmed that the CO conversion rate of powdered $CuCe_{0.75}Zr_{0.25}O_\delta$ catalyst increased rapidly from the beginning of the process to the self-combustion state due to the strong exothermic reaction under a 15% CO/air atmosphere, and the limits of a lean combustion were also obtained at various flow rates [13].

To contribute to the development of new technologies for CO catalytic combustion, it is important to investigate the scaling methodology from laboratory to industrial conditions in-depth. Honeycomb ceramic (HC) catalysts, which consist of narrow, straight, parallel channels separated by thin walls, are very promising because they provide a low pressure drop, low diffusion resistance and better mass and heat transfer in the channels than powder catalysts. Here, we prepared a new $CuCe_{0.75}Zr_{0.25}O_\delta$/HC catalyst by the sol-gel and impregnation methods coupled with the induction mechanism of different reactant concentrations to investigate the transient changes during CO self-combustion. The activity test was mainly carried out under different off-gas concentrations (0–15 vol% CO, 3–15 vol% O_2 and 10–40 vol% CO_2) via the temperature-programmed oxidation of CO together with a forward-looking infrared radiometer (CO-TPO + FLIR). In particular, the high-temperature durability of the $CuCe_{0.75}Zr_{0.25}O_\delta$/HC catalyst was also inspected by CO-TPO and scanning electron microscopy (SEM) with energy dispersive X-ray spectroscopy (EDX). The CO reaction detailed mechanisms, such as the adsorption and rapid transform-reaction pathways of reactants on the different active sites, were determined using in situ infrared (in situ IR) Fourier transform spectroscopy.

2. Experimental methods

2.1. Catalyst preparation

The $CuCe_{0.75}Zr_{0.25}O_\delta$ powdered catalyst was prepared by the sol-gel method using $Cu(NO_3)_2{\cdot}3H_2O$, $Ce(NO_3)_3{\cdot}6H_2O$ and $Zr(NO_3)_4{\cdot}5H_2O$ dissolved fully in 70 mL of ethanol at 80 °C. The Cu:Ce:Zr molar ratio of 4:3:1 was selected according to the structure optimization published by our previous work [3]. Oxalic acid solution (0.24 mol/L) was used as a pore former and was added quickly to the aforementioned nitrate solution with stirring to evaporate the ethanol and to fully dissolve all components until a gel was formed at 80 °C for approximately 6 h. After aging for approximately 48 h at room temperature, the gel was dried at 105 °C for 12 h and then calcined at 550 °C for 2 h in air. The obtained powdered catalyst was labeled $CuCe_{0.75}Zr_{0.25}O_\delta$.

To prepare the $CuCe_{0.75}Zr_{0.25}O_\delta$/HC catalyst, the quantities of polyethylene glycol (PEG2000), pseudo boehmite, and citric acid were added to water (m(H_2O):m(citric acid):m(PEG2000):m(pseudo boehmite) = 5:1.4:0.6:3) and heated at 80 °C for 3 h via continuous stirring, forming a homogeneous sticky liquid. The $CuCe_{0.75}Zr_{0.25}O_\delta$ powdered catalyst was added to the sticky liquid and then formed a 30 wt% catalyst slurry after stirring for 3 h. The undefiled ceramic honeycomb tubes (25 mm × 25 mm × 100 mm) were immersed in the catalyst slurry for 2 h and blown with compressed air to remove the excess solution in the channel. After drying at 110 °C for 12 h, this material was calcined at 550 °C for 4 h in air. A weighing method was used to ensure the actual load of the $CuCe_{0.75}Zr_{0.25}O_\delta$ catalyst reached a predetermined desired amount (30 wt%) by repeating the above process. The obtained catalyst is denoted as a $CuCe_{0.75}Zr_{0.25}O_\delta$/HC catalyst.

2.2. Characterization

X-ray powder diffraction (XRD) spectra were recorded on an XD-3-automatic instrument (PERSEE) equipped using a Cu Kα radiation source (40 kV, 200 mA, and λ = 1.5418 Å). The patterns were collected over a diffraction angle (2θ) range of 10°–80° with a step length of 0.02° at a scanning rate of 4°/min. The elemental compositions of the catalysts were determined by X-ray fluorescence (XRF) analysis on an Epsilon l Research and a Power 4200 scanning XRF spectrometer. SEM images with EDX (Oxford X-MAX) were performed on a TESCAN MIRA3 scanning electron microscope.

In situ infrared (IR) spectroscopy experiments were conducted on a Bruker Tensor 27 spectrometer equipped with a highly sensitive

mercury cadmium telluride (MCT) detector cooled by liquid nitrogen. Self-supporting disks prepared from the sample were suspended in a quartz holder and then mounted in a high-temperature infrared (IR) cell. The transmission mode is employed in situ IR experiments. Before the experiment, approximately 20 mg of the sample was pretreated in N_2 (80 mL/min) at 400 °C for 1 h and cooled to the desired temperature for collection of a reference spectrum. The three conditions of the reaction gas mixture (10 vol% CO; 10 vol% CO + 10 vol% O_2; and 10 vol % CO + 10 vol% O_2 + 20 vol% CO_2, N_2 balance) were fed to the sample at a total flow rate of 80 mL/min at room temperature for 0.5 h and then purged with N_2 for 40 min to avoid the physical adsorption of $CO/O_2/CO_2$. For each temperature interval (from room temperature to 400 °C), a series of time-dependent spectra from in situ IR of the reaction on the sample were sequentially recorded with a resolution of 4 cm^{-1} and 64 scans were conducted.

2.3. Catalytic activity testing

The CO-TPO experiments were performed in a flow-type temperature-controlled apparatus for continuous operation under atmospheric pressure. The experimental setup for CO self-sustained combustion included a catalytic combustion reactor, continuous flow gas supply systems and gaseous analytical systems, as shown in Fig. 1. The $CuCe_{0.75}Zr_{0.25}O_\delta$/HC catalyst was packed inside a fixed-bed quartz tube reactor with an inner diameter of 2.5 cm, and the total flow rate of reactants was set at 0.5 L/min. The same size of the air distribution plate (d = 2.5 cm) was placed in the reactor, located on the front of the catalyst sample to realize a uniform distribution of reactants. The flow rates of CO, O_2, CO_2 and N_2 were controlled by mass flow controllers with a full-scale measurement accuracy of ± 1%, which are shown as MFC1, MFC2, MFC3 and MFC4, respectively. Temperature-programmed ignition of CO was carried out under heating (5 °C/min) from room temperature in the gas mixture. One K-type thermocouple was located between the reactor wall and oven wall to control the oven temperature, and the other was immersed inside the front of catalyst bed to measure the temperature continuously. The temperature distributions of the reactor surface were obtained via a forward-looking infrared radiometer (FLIR, T640, USA), with a certain glass emission rate (0.87). During each test, the steady self-sustained catalytic combustion of CO was determined by the temperature of the reactor wall varying within a range of ± 2 °C for 10 min, which is obviously higher than room temperature. An online gas measurement system (QGS-08, Maihak) was employed to detect the effluent concentration of CO, O_2 and CO_2.

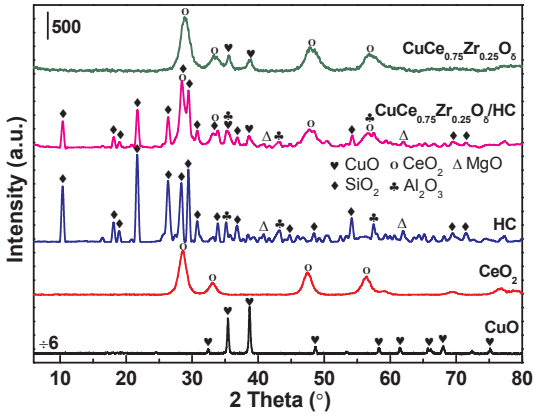

Fig. 2. XRD patterns of the $CuCe_{0.75}Zr_{0.25}O_\delta$/HC catalyst.

3. Results and discussion

3.1. XRD and XRF analysis

Fig. 2 shows the XRD patterns of the $CuCe_{0.75}Zr_{0.25}O_\delta$/HC catalyst, CuO, CeO_2, and HC samples. Compared with the HC sample, the width of the SiO_2 diffraction peaks (2θ = 28.4°, 29.5°, 33.8 and 48.4°; PDF Nos. 83–1833 and 82–1403) of the $CuCe_{0.75}Zr_{0.25}O_\delta$/HC catalyst broadened, and the intensity weakened due to the existence of CeO_2 (2θ = 28.5°, 33.1° and 47.4°; PDF No. 34–0394). The diffraction peaks of cubic CeO_2 with a fluorite structure in the $CuCe_{0.75}Zr_{0.25}O_\delta$/HC catalyst shifted to increased 2θ values as a function of the overlap between SiO_2 and CeO_2. The similar two weak diffraction peaks located at 2θ values of 35.5° and 38.7° were assigned as the CuO crystal phase in the $CuCe_{0.75}Zr_{0.25}O_\delta$ powdered and $CuCe_{0.75}Zr_{0.25}O_\delta$/HC catalysts. Compared with the XRD patterns between powdered $CuCe_{0.75}Zr_{0.25}O_\delta$ and $CuCe_{0.75}Zr_{0.25}O_\delta$/HC, no obvious difference in structure could be observed. The XRF results suggest that the $CuCe_{0.75}Zr_{0.25}O_\delta$/HC catalyst contained 32.89 wt% SiO_2, 26.01 wt% Al_2O_3, 9.24 wt% MgO, 10.64 wt % CuO, 16.50 wt% CeO_2, and 3.72 wt% ZrO_2. The actual capacity of the $CuCe_{0.75}Zr_{0.25}O_\delta$ powdered catalyst was 30.86 wt% on HC, which is slightly higher than the theoretical value of 30 wt%.

3.2. Catalytic activity testing

Fig. 3 displays the transient curves of the CO combustion with different CO concentrations over the $CuCe_{0.75}Zr_{0.25}O_\delta$/HC. The

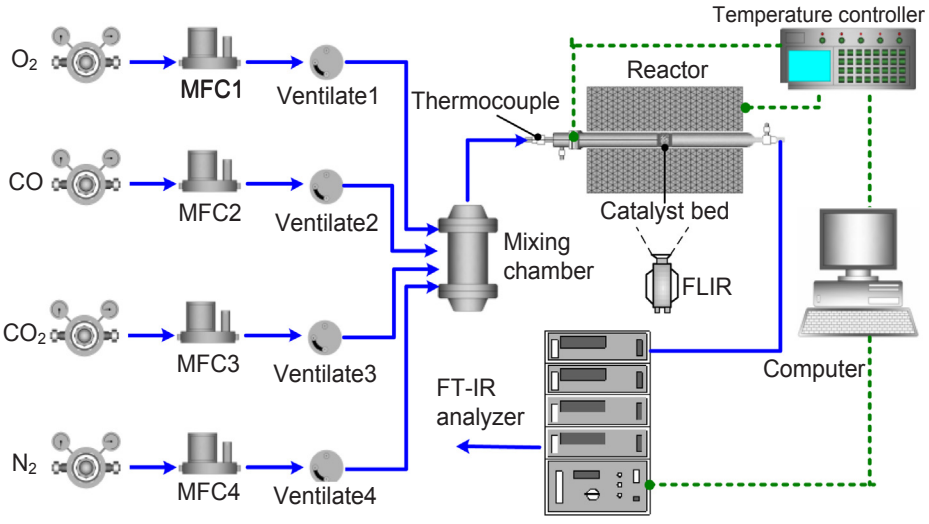

Fig. 1. Schematic of the experimental apparatus for CO self-sustained combustion.

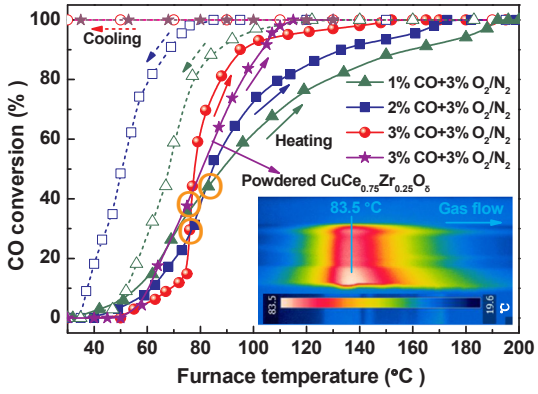

Fig. 3. Ignition curves of CO and distribution of two-dimensional (2D) temperature field under $CuCe_{0.75}Zr_{0.25}O_{\delta}$/HC (1 vol%, 2 vol%, 3 vol% CO + 3 vol % O_2/N_2).

$CuCe_{0.75}Zr_{0.25}O_{\delta}$/HC catalyst revealed the three main steps to realize CO self-combustion under heated conditions. The first step refers to a slow induction process at the temperature of CO catalytic ignition (T_{15}), corresponding to CO conversions below 15%. Herein, the reaction was controlled by the kinetic regime due to the partial pressures of CO and O_2, which had an important effect on the reaction rate [10,14]. The second phase can be described as a light-off process, and the reaction rate depended on the internal and external diffusion instead of kinetic diffusion in porous HC materials [15,16]. The exothermic reaction of CO combustion generated local hot active centers on the catalyst surface in this step, and the rate of heat generation was much higher than that of heat dissipation, thus inducing a rapidly increasing CO conversion curve. Here, the light-off temperature of the CO catalytic reaction (T_{90}), corresponding to the temperature at which CO conversion, was 90%. The third stage included both external diffusion and thermal diffusion processes, which occurred on the adjacent and limited active sites of the $CuCe_{0.75}Zr_{0.25}O_{\delta}$/HC catalyst. Evidently, CO ignition can be ascribed to such a process where a temperature-triggered kinetic transition from the low-rate steady state regime to a high-rate steady state occurred, enabling 100% CO conversion (corresponding to the temperature defined as T_{100}).

Changes in the curve shape during transient ignition can be observed as a function of CO concentration. As shown in Fig. 3, the CO conversion rate decreased during the induction process, with the CO concentration in the atmosphere increasing from 1 vol% to 3 vol%. Such a slow reaction rate obtained at high CO content may be partially caused by local mass transfer limitations, resulting in a slow update frequency of the reactants. This rate is probably also attributable to the high concentration of CO adsorbing easily on the Cu-Ce active surface sites, but it is difficult to react fully and promptly to form CO_2 at low temperature ($< T_{15}$). A similar phenomenon can also be evidenced by other groups, given that the oxygen vacancies occupied by excessive CO result in self-poisoning [12]. This dilemma did not change significantly until it entered the second stage (from T_{15} to T_{90}) with temperature. Once the accumulation of heat promoted ignition, the adsorbed CO molecules reacted rapidly with lattice oxygen to yield CO_2, and then the created oxygen vacancies are immediately replenished by gaseous O_2 dissociation on the catalyst surface, in which case the catalytic cycle is maintained [10]. This phenomenon will be testified in the subsequent section of in situ IR spectroscopy analysis. Under the increased CO content in the atmosphere, the ignition curve at the second stage had a larger slope than that at the decreased CO content due to CO self-poisoning during the induction process and accumulating heat. Therefore, the ignition curves intersect each other at 76 °C between 2 vol% and 3 vol% CO, 77 °C between 1 vol% and 3 vol% CO, and 82 °C between 1 vol% and 2 vol% CO. Frank-Kamenetskii found that a similar phenomenon produced a critical point during the catalytic oxidation process and defined the conditions for catalytic ignition [17]. Entering the third stage, a high-rate steady state cannot be achieved until a long process occurred because the heat released continuously after a sudden self-acceleration of CO oxidation over the catalyst surface.

As the CO concentration increased from 1 vol% CO to 3 vol% CO, the induction process ($< T_{15}$) shifted toward a decreased CO reaction rate, while the light-off process (T_{15}-T_{90}) had a rapid ignition for the CO oxidation reaction. The former is attributed to CO self-poisoning on the active sites at high CO concentrations, which is controlled by kinetics. The later transient change occurs with a sudden self-acceleration rate, which is controlled by internal and external diffusion; this rate is due to a rapid increase in the temperature of the exothermic CO combustion reaction, and it cannot dissipate in a timely manner from the catalyst bed. Moreover, the light-off process had a high gas diffusivity $D_v \propto T^{1.81}$ and high mass-transfer coefficient $K_s = (D_v \cdot S)^{1/2}$, where T denotes temperature and S denotes update frequency [18].

Upon cooling feeding, the curve (dashed lines) followed a reverse transition from the third to the first step. At CO concentrations of 1 and 2 vol%, the cooling curves of the CO conversions shifted toward low temperatures compared with the heating curves. This hysteresis can be attributed to the exothermic effect and accumulated heat of the CO combustion on the catalyst bed so that the controlled temperature decreased below the ignition temperature without influencing the reaction rate. Because of the fast mass and heat transfers on the gas–solid phase interface, the self-sustained combustion of CO can be achieved at 3 vol% CO content even after the heating stopped and the controlled temperature was maintained at room temperature. After the balance of the heat transfer from the catalyst to the air via the wall of the quartz tube, a stable two-dimensional temperature distribution was also detected, with the high-temperature zone maintaining a temperature of 83.5 °C. In order to compare the activity of $CuCe_{0.75}Zr_{0.25}O_{\delta}$/HC, the same reaction conditions (3 vol% CO + 3 vol% O_2/N_2 at 0.5 L/min, 0.2 g) are also carried out for $CuCe_{0.75}Zr_{0.25}O_{\delta}$ powered catalyst. It could be found that the powered $CuCe_{0.75}Zr_{0.25}O_{\delta}$ achieves complete CO conversion (T_{100}) at 115 °C, which is lower than that of $CuCe_{0.75}Zr_{0.25}O_{\delta}$/HC catalyst ($T_{100}$ for 152 °C).

Fig. 4 describes the effect of high CO concentration on self-sustained combustion behavior over the $CuCe_{0.75}Zr_{0.25}O_{\delta}$/HC under the 10 vol% O_2/N_2 condition. Due to the sharp exothermic CO combustion reaction, both the induction and light-off processes of the heating curves decreased with CO content, corresponding to the curves shifting toward the low-temperature direction evidenced by T_{90}, which was 107 °C for 5 vol% CO, 95 °C for 10 vol% CO, and 86 °C for 15 vol% CO. However, the third stage should take a longer time to reach steady state with CO content, viz. T_{100} is 128 °C for 5 vol% CO, 136 °C for 10 vol% CO, and 146 °C for 15 vol% CO. Hence, the three intersection points appeared at 102 °C between 10 vol% and 15 vol% CO, 116 °C between 5 vol% and

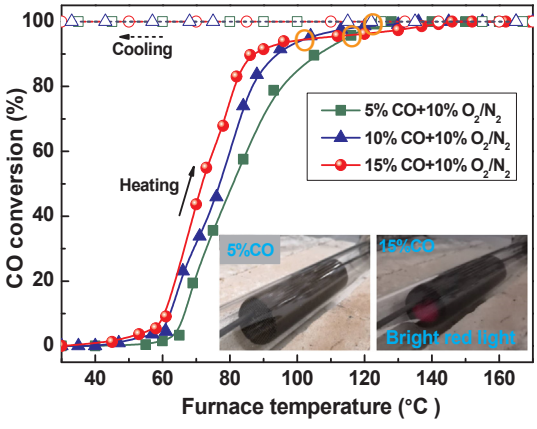

Fig. 4. CO-TPO under a $CuCe_{0.75}Zr_{0.25}O_{\delta}$/HC catalyst (5 vol%, 10 vol%, and 15 vol% CO + 10 vol% O_2/N_2).

15 vol% CO and 122 °C between 10 vol% and 15 vol% CO. Both external and thermal diffusion can dominate such a process because the high concentration of CO adsorbs easily and converts rapidly under a sudden self-acceleration on the limited hot active sites so that the speed of thermal diffusion on the catalyst surface cannot catch up with that of the strong local exothermic release. Typical photographs of the CO self-sustained combustion are displayed in Fig. 4. The luminous zone can only be observed in the front of the $CuCe_{0.75}Zr_{0.25}O_{\delta}$/HC bed because of the thermal radiation at 15 vol% CO, although self-sustained combustion was also achieved at the 5 vol% CO condition. The reason may be that the rapid mass and heat transfer were sufficient to sustain CO self-sustained combustion in the front of the $CuCe_{0.75}Zr_{0.25}O_{\delta}$/HC bed; thus, it did not need to react along the gas flow.

Fig. 5 illustrates the activities of $CuCe_{0.75}Zr_{0.25}O_{\delta}$/HC with different concentrations of O_2 under 5 vol% CO/N_2 conditions. The curve of the CO conversion shifts toward the lower temperature direction with increasing O_2 concentration, and the T_{100} values are 155 °C, 145 °C, and 140 °C, corresponding to the O_2 contents at 5 vol%, 10 vol% and 15 vol %, respectively. Evidently, the increasing partial pressure of O_2, which was compensated by a decrease in the partial pressure of N_2, promoted the CO catalytic combustion because a substantial amount of oxygen reacted instantly with the preadsorbed CO molecules on the active sites [19,20]. When the CO self-sustained combustion was maintained at 5 vol%, 10 vol% and 15 vol% O_2, a nearly identical temperature distribution was formed, and the high-temperature region reached 113 ± 1 °C, indicating that the temperature gradients were mainly determined by the CO concentration rather than the O_2 concentration.

Fig. 6 shows the conversion curves of CO self-combustion with different CO_2 concentrations at a 5 vol% CO + 5 vol% O_2/N_2 atmosphere over $CuCe_{0.75}Zr_{0.25}O_{\delta}$/HC. As the CO_2 concentration increased, the profile of the CO conversion shifted toward a high-temperature direction upon heating feeding, and both induction and light-off processes lasted a long time. The inhibition effect should arise from the competitive adsorption between the CO_2 and CO/O_2 on the active sites, which was verified by in situ IR spectroscopy analysis. The external thermal diffusion processes (the third stage), however, decreased with CO_2 content, corresponding to the ΔT values (defined as T_{100}-T_{90}) at 37 °C for 10 vol% CO_2, 35 °C for 20 vol% CO_2, 32 °C for 30 vol% CO_2, and 30 °C for 40 vol% CO_2. Moreover, the high-temperature region maintained within the catalyst bed decreased from 112 °C to 103 °C, corresponding to the CO_2 concentration increasing from 10 vol% to 40 vol%. This is because the specific heat capacity of the CO_2 (37.00 J/(mol·K)) was higher than that of the N_2 (29.12 J/(mol·K)), thus resulting in a large heat transfer and loss to air.

The power rate law expressions of the reaction rates under the partial pressure of CO, O_2 and CO_2 are also carried out to investigate the effect reactants concentration on CO catalytic combustion, as shown in Fig. 7. The kinetic data of the CO reaction rates under various partial pressures of CO, O_2 and CO_2 is calculated by the activity results (Figs. 4, 5 and 6). In order to eliminate both internal and external mass transfer resistance, the CO conversion is controlled below 20% under gas flow rate at 0.5 L/min. Reaction temperatures of 65 °C, 60 °C and 90 °C are employed to account for the different reaction rates in the kinetic region, corresponding to the partial pressures of CO, O_2 and CO_2, respectively. The obtained power rate law expression follows: $r = 8.57 \times 10^{-7} \times P_{CO}^{0.99} P_{O2}^{0.35} P_{CO2}^{-0.48}$, which further confirms that the increasing partial pressures of CO and O_2 promote the CO reaction rates but CO_2 acted as an inhibitor.

3.3. Long-term stability testing

A time-on-stream study was carried out to assess the $CuCe_{0.75}Zr_{0.25}O_{\delta}$/HC catalyst stability under the conditions of 15 vol% CO + 15 vol% O_2/N_2. Fig. 8(A) clearly shows stable CO combustion during the 200 h test, and the high-temperature region of the reaction was located in the front of the catalyst bed after the balance of heat conduction and heat transfer to air. The axial temperature distribution profile (Fig. 8(b)) shows that the hot zone migrated downstream by a distance of 0.6 cm from its initial position after 150 h, with nearly no further movement observed during the other 50 h run. Despite the partial deactivation of catalysts, the high-temperature region was always maintained at 220 ± 2 °C along with the test.

The activities of the fresh and used $CuCe_{0.75}Zr_{0.25}O_{\delta}$/HC catalysts were also evaluated after a 200 h run. Before the test, it can be seen in Fig. 9 that the catalyst used became slightly black after the 200 h run. Compared to that of the fresh catalyst, the curve of the CO conversion for the used catalyst shifted toward high temperatures during the heating process, corresponding to a T_{100} at 150 °C (142 °C for the fresh catalyst). Although the activity of the catalyst decreased relatively, CO self-sustained combustion can still be achieved. After a 2 h regeneration process at 400 °C under an air atmosphere, the CO conversion for the regenerated catalyst basically agrees with the results of the fresh catalyst at elevated temperature (Fig. 9) corresponding to T_{100} = 143 ± 2 °C (142 °C for the fresh catalyst). This suggests that the $CuCe_{0.75}Zr_{0.25}O_{\delta}$/HC catalyst used after a 200 h time-on-stream test can remove carbon deposition by the air oxidation method, and thus, the activity can nearly recover to the level of the fresh catalyst.

To probe the nature of the slight deactivated catalysts, SEM with EDX analysis was performed, with the micrographs of fresh and used $CuCe_{0.75}Zr_{0.25}O_{\delta}$/HC displayed in Fig. 10. The powdered $CuCe_{0.75}Zr_{0.25}O_{\delta}$ catalyst was loaded onto the HC tube surface, which dispersed well with strong adhesion (Fig. 10(A)). For the catalyst used after the 200 h run, however, small flocky particles can be observed in the sample (the axial distance of the HC < 0.5 cm) (Fig. 10(B)). The EDX spectra (point 2) revealed that the carbon content was approximately 6.85 wt%, whereas no carbon was detected on the fresh sample (point 1), indicating that the deactivation results from the carbon deposition on the catalyst surface.

3.4. In situ IR spectroscopy analysis

To further demonstrate the intermediates in CO oxidation, in situ IR spectroscopy was first conducted under a N_2 flow of 80 mL/min at 30 °C to sweep the gaseous CO for 40 min. Before the in situ IR spectroscopy, the catalyst was pretreated with N_2 at 300 °C, pre-adsorbed with 10 vol % CO/N_2, 10 vol% CO + 10 vol% O_2/N_2 or 10 vol% CO + 10 vol% O_2 + 20 vol% CO_2/N_2. As shown in Fig. 11, IR bands can be observed in three spectral zones that generally relate to the physical adsorption of CO_2 (2400–2200 cm^{-1}), the formation of carbonyl species (2200–2000 cm^{-1}) and the formation of carbonates (1800–1200 cm^{-1}). When gaseous CO first coordinated to the copper sites in the $CuCe_{0.75}Zr_{0.25}O_{\delta}$/HC to form carbonyls, the C-O stretching frequency shifted compared to that of the original CO measured in the

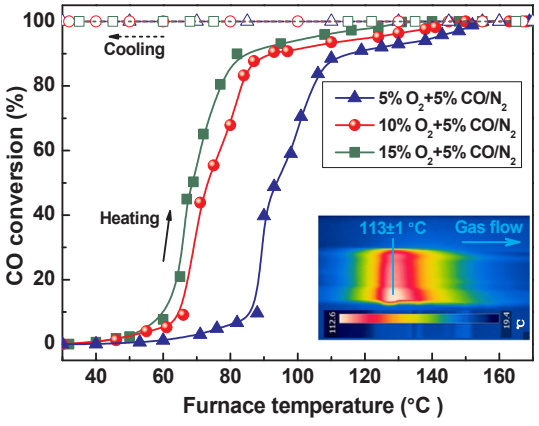

Fig. 5. CO-TPO under a $CuCe_{0.75}Zr_{0.25}O_{\delta}$/HC catalyst (5 vol%, 10 vol%, and 15 vol% O_2 + 5 vol% CO/N_2).

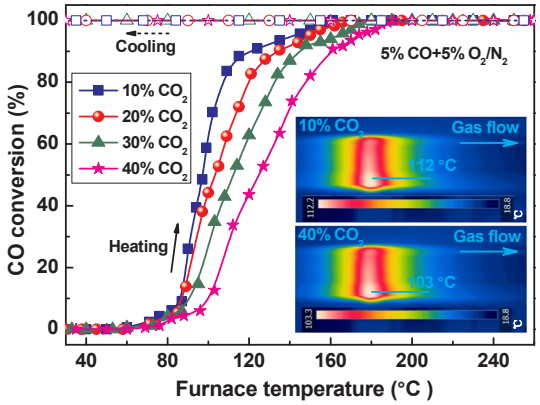

Fig. 6. CO-TPO under a $CuCe_{0.75}Zr_{0.25}O_{\delta}$/HC catalyst (10 vol%, 20 vol%, 30 vol %, and 40 vol% CO_2 + 5 vol% CO + 5 vol% O_2/N_2).

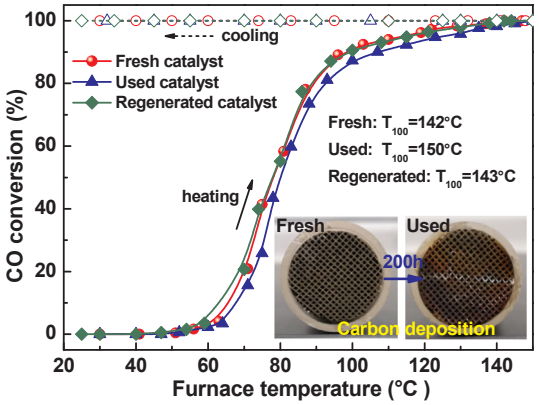

Fig. 9. The activity experiments of fresh, used and regenerated $CuCe_{0.75}Zr_{0.25}O_{\delta}$/HC catalysts for 15 vol% CO + 15 vol% O_2/N_2.

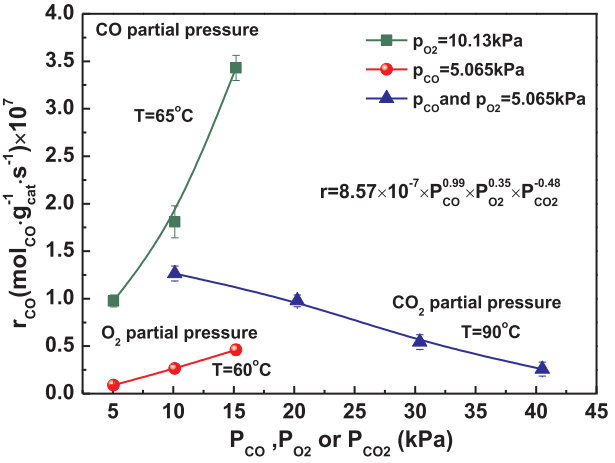

Fig. 7. Kinetic results of CO oxidation over the $CuCe_{0.75}Zr_{0.25}O_{\delta}$/HC.

gas phase (2171 and 2115 cm^{-1}, respectively). Carbonyls [Cu^{+}–CO] were formed as active intermediates corresponding to the peak located at 2108 cm^{-1}, which exhibited high stability due to the simultaneous formation of and synergy between the σ bonds and π-back-bonding between the CO and copper cations [21]. The carbonyl peaks, overlapped by those of the gaseous CO, cannot be observed until the gaseous CO was swept by the N_2. CO also chemisorbed with oxygen onto the Cu-Ce active sites, giving rise to carboxylate (1509 cm^{-1}) and carbonate (1330 cm^{-1}) species [22]. Two bands (2382 and 2347 cm^{-1}) were identified by the P and R branches of physically adsorbed CO_2 in the ground vibrational state, which confirms that CO oxidation occurred even at room temperature. The IR band areas of carbonyl and carbonate species after N_2 sweeping for 40 min are also listed in Fig. 11D. It should be noted that the competitive adsorption among CO/O_2 and CO_2 on Cu-Ce sites was apparent for the catalyst. Hence, the carbonyl peaks under 10% CO/N_2 pre-adsorption were higher than those after 10% CO + 10% O_2/N_2 pre-adsorption, whereas the carbonyls formed after 10% CO + 10% O_2 + 20% CO_2/N_2 pre-adsorption were quite small. In contrast, both O_2 and CO_2 additions promoted the formation of carbonates, whereas the carbonyl peaks formed after 10% CO/N_2 pre-adsorption became weak.

After N_2 sweeping for 40 min at room temperature, the temperature-programmed oxidation was carried out at a heating rate of 10 °C/min. As displayed in Fig. 12, a temperature increase led to the band intensity at 2108 cm^{-1}, which is related to carbonyls, rapidly decreasing, whereas the bands at 1509 and 1330 cm^{-1}, which are related to carbonates, decreased slowly. The same IR peak at 1270 cm^{-1} occurs after 300 °C in the different reaction conditions, attributed to the baseline drift of HC materials with the temperature increasing. The catalytic activity of copper-cerium-based materials toward CO oxidation was largely affected by two significant factors: the Cu active sites and the surface active oxygen species [23]. CO was preferentially adsorbed on Cu active sites to yield [Cu^{+}–CO] complexes due to the antibonding π-orbital of Cu^{+} [24]. The adsorbed CO interacted with neighboring lattice oxygen after 50 °C in a strongly exothermic

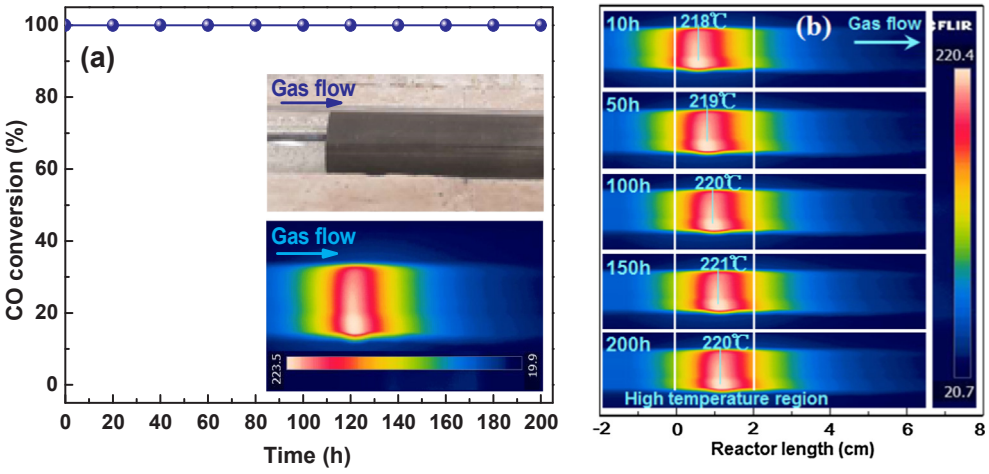

Fig. 8. (a) The durability test and the distribution of temperature (inset) and (b) the distribution of temperature over the $CuCe_{0.75}Zr_{0.25}O_{\delta}$/HC catalyst (15 vol% CO + 15 vol% O_2/N_2).

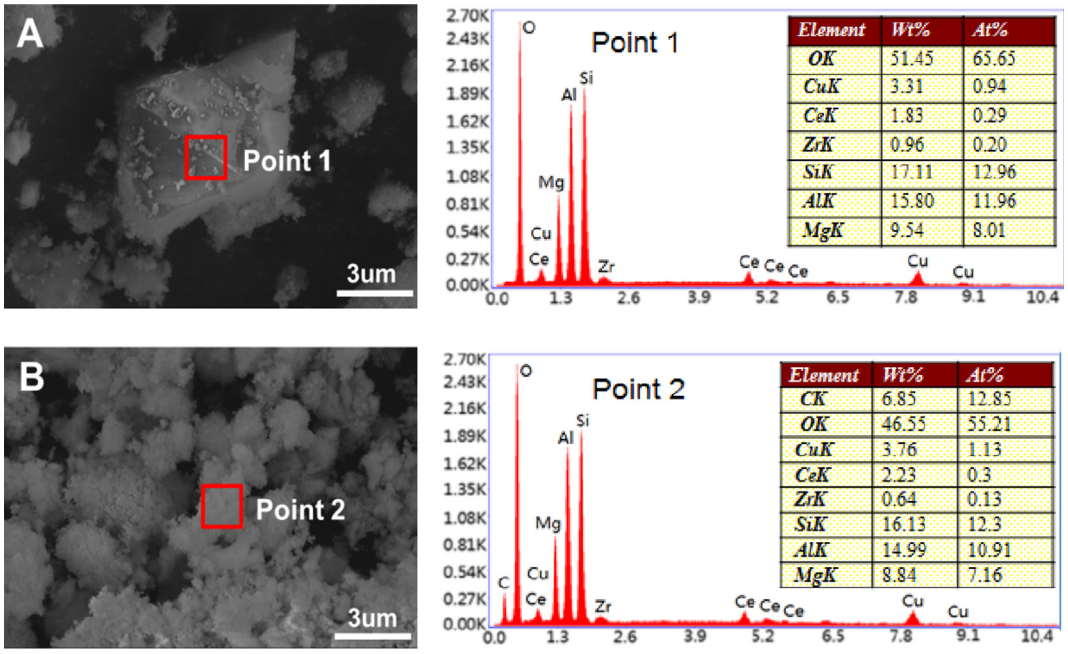

Fig. 10. SEM + EDX spectra of fresh (A) and used (B) $CuCe_{0.75}Zr_{0.25}O_8$/HC catalysts.

reaction, forming CO_2 then releases into atmosphere, following the M-K mechanism. CO was also adsorbed with active oxygen on the Cu-Ce active sites to produce carbonates, assigned to the L-H mechanism as less important step. Further decomposition of carbonates after 150 °C to form CO_2 involved the uptake of the activated oxygen, and therefore, abundant active oxygen formed after 10 vol% CO + 10 vol% O_2/N_2 promoted this process.

In situ IR spectroscopy was also carried out under 10% CO + 10% O_2/N_2 and 10% CO + 10 vol% O_2 + 20 vol% CO_2/N_2 continuous streams to identify the CO ignition process and inhibition of CO_2. The spectra from IR spectroscopy (Fig. 13) display intense bands at 2171 and 2115 cm^{-1} assigned to gaseous CO and slight bands at 1509 and 1330 cm^{-1} related to carbonates, respectively. Under the 10% CO + 10% O_2/N_2 atmosphere, the CO band decreased rapidly, and the

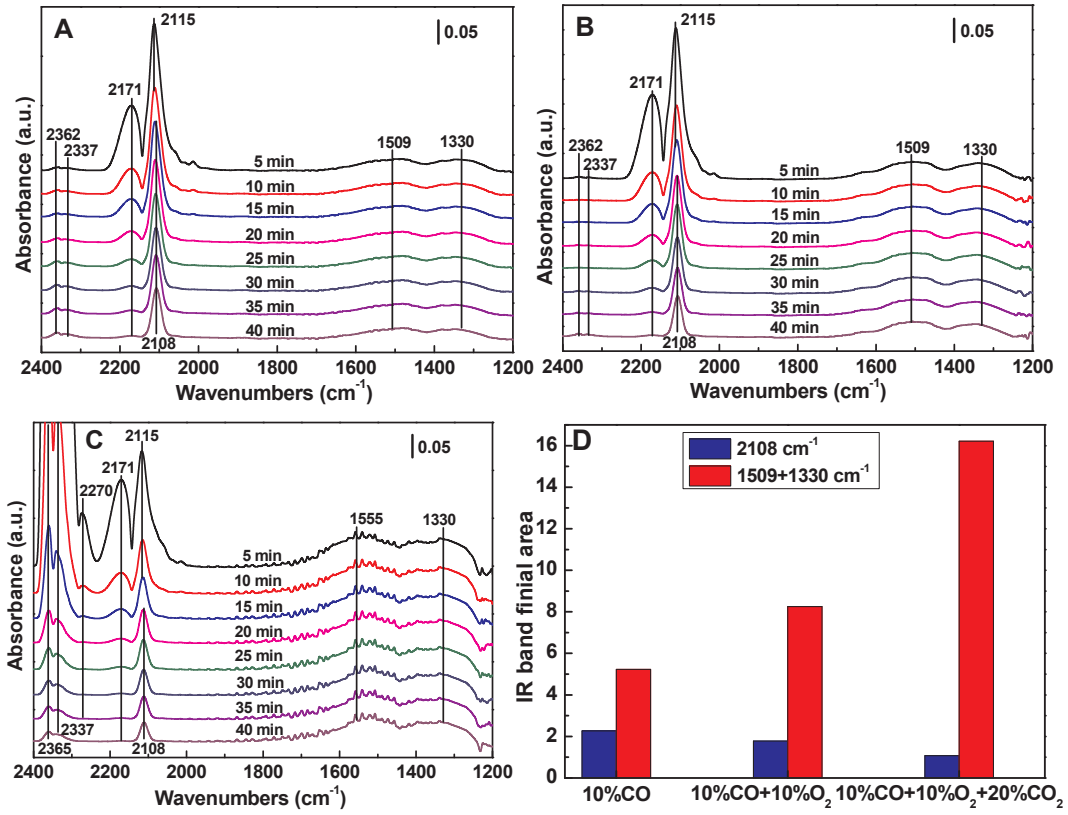

Fig. 11. Variations in carbonyls, carbonates and physically adsorbed CO_2 during the N_2 sweeping process after (A)10 vol% CO/N_2, (B) 10 vol% CO + 10 vol% O_2/N_2, and (C) 10 vol% CO + 10 vol% O_2 + 20 vol% CO_2/N_2 pre-adsorption at 30 °C.

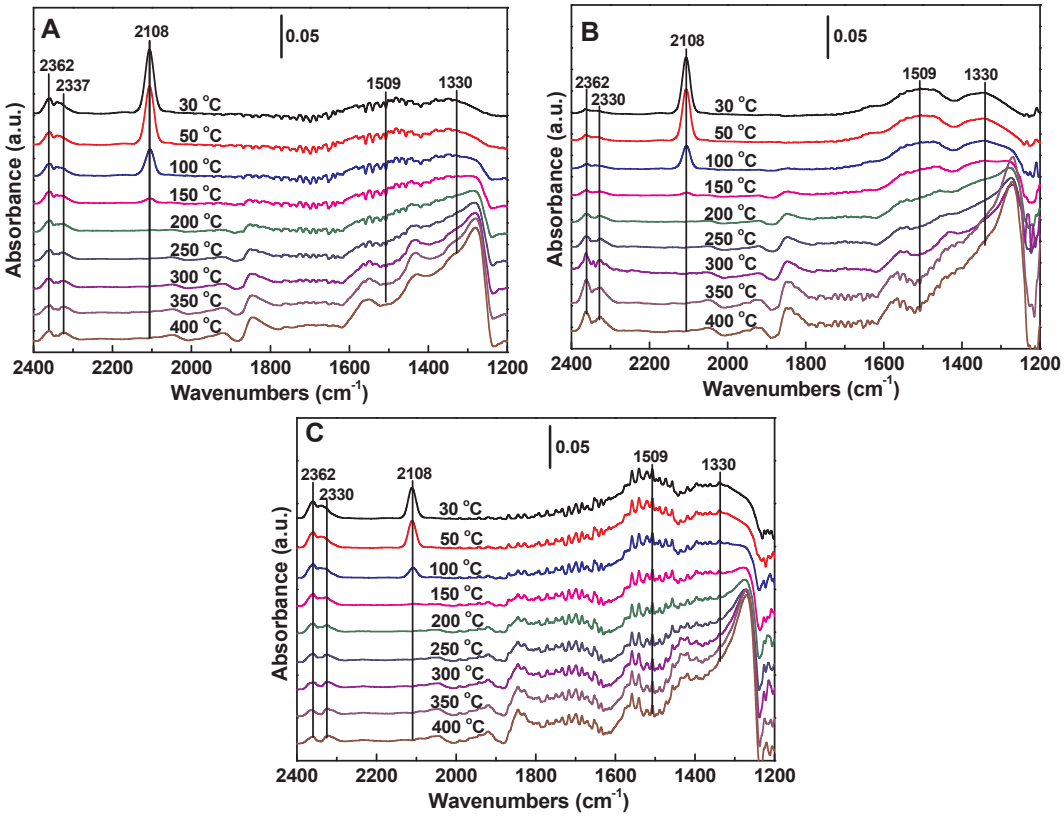

Fig. 12. Temperature-programmed oxidation process after the N_2 sweeping process: (A) 10 vol% CO/N_2, (B) 10 vol% CO + 10 vol% O_2/N_2, (C) 10 vol% and CO + 10 vol% O_2 + 20 vol% CO_2/N_2.

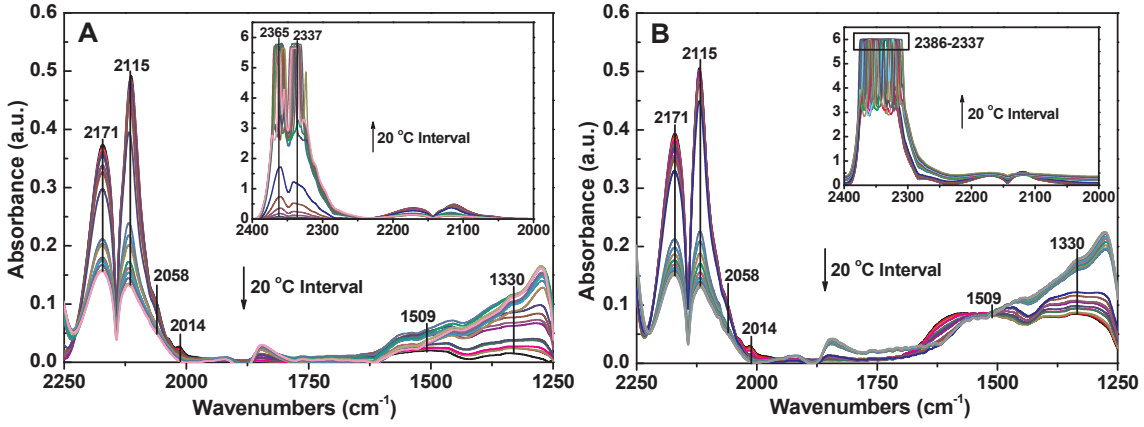

Fig. 13. Spectra from in situ IR for the CO ignition (30–400 °C) under (A) 10 vol% CO + 10 vol% O_2/N_2, and (B) 10 vol% CO + 10 vol% O_2 + 20 vol% CO_2/N_2 continuous streams.

carbonyl band disappeared as the temperature reached 200 °C, whereas the CO_2 bands at 2365 and 2337 cm^{-1} grew rapidly instead, confirming the generation of transient changes and then reaching self-sustained combustion (Fig. 13A). Here, the ignition temperature in the IR cell was much higher than that in the powder-filled tube reactor, given that the pressed-powder wafer was unfavorable for the accumulation of heat during the exothermic reaction. In contrast, the CO_2 addition obviously inhibited the CO oxidation under the 10 vol% CO + 10 vol% O_2 + 20 vol% CO_2/N_2 atmosphere, leading to CO ignition at 240 °C (Fig. 13B). The CO_2 formed from the oxidation between the CO and O_2 releases to the atmosphere, which is an irreversible process for CO self-sustained combustion. The addition of CO_2 (10 vol%–40 vol%) in the initial reactants, however, the competitive adsorption to form carbonate species among CO/O_2 and CO_2 on Cu-Ce sites was apparent for the catalyst, inhibiting the normal oxidation of CO, in agreement with kinetic results.

In situ IR spectroscopy revealed that M-K mechanism is dominant where CO preferentially adsorbs linearly at Cu^+ active sites and then reacts with lattice oxygen of copper oxides and/or Cu–O–Ce oxides to form CO_2 at low temperature (see Scheme 1). The presence of CO_2 in the gas phase can inhibit the oxidation of CO since unreacted CO and CO_2 can competitively adsorbed on the active sites. The other reaction related to L-H mechanism is less important on the $CuCe_{0.75}Zr_{0.25}O_8$/HC catalyst, which involves the adsorbed CO and adsorbed oxygen on the Cu-Ce solid solutions to form carbonate species, following by the yield of CO_2. This can be also verified via kinetic results by our pervious study [10].

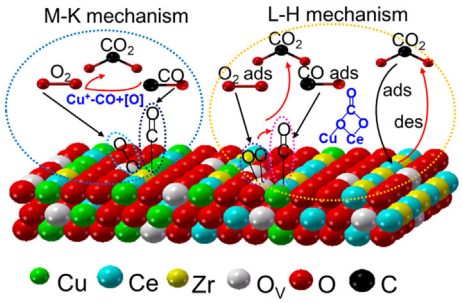

Scheme 1. The detailed reaction mechanisms of CO oxidation over the $CuCe_{0.75}Zr_{0.25}O_{\delta}$/HC catalyst.

4. Conclusions

In this study, the $CuCe_{0.75}Zr_{0.25}O_{\delta}$ powdered sample is well dispersed on the HC tube with a loading ratio of 30.86 wt% on the $CuCe_{0.75}Zr_{0.25}O_{\delta}$/HC catalyst. As the CO concentration increases from 1 to 3 vol% CO, the induction process ($< T_{15}$) shifts toward slower CO conversion (self-poisoning), while the light off process (T_{15}-T_{90}) turns to rapid ignition ((self-acceleration) for the CO oxidation reaction. Then, CO self-sustained combustion is realized due to transient heat release at 3 vol% CO + 3 vol% O_2/N_2. After a 200 h time-on-stream test, the $CuCe_{0.75}Zr_{0.25}O_{\delta}$/HC catalyst maintains a high thermal stability and removes a slight deposition of the carbon by air oxidation, and thus, the activity almost recovers to the level of the fresh catalyst. Increasing CO and O_2 concentrations promoted CO self-sustained combustion, but the inhibition effect occurs with increasing CO_2 concentrations. The M-K mechanism is a critical reaction pathway for the CO self-combustion reaction; specifically, CO preferentially adsorbs onto the Cu^+ over the catalyst, interacting with lattice oxygen in a strongly exothermic reaction. Additionally, the competitive adsorption of CO/O_2 and CO_2 on Cu-Ce active sites is obtained, followed by the L-H mechanism.

Declaration of Competing Interest

The authors declare that they have no known competing financial interests or personal relationships that could have appeared to influence the work reported in this paper.

Acknowledgments

We gratefully acknowledge the financial support from the National Natural Science Foundation of China (51776216, 51736010) and the Transformational Technologies for Clean Energy and Demonstration, Strategic Priority Research Program of the Chinese Academy of Sciences, Grant No. XDA21040500.

References

[1] Arens M, Worrell E, Schleich J. Energy intensity development of the German iron and steel industry between 1991 and 2007. Energy 2012;45:786–97.
[2] Li S, Wei XL, Yu LX. Numerical simulation of off-gas formation during top-blown oxygen converter steelmaking. Fuel 2011;90:1350–60.
[3] Zhao RZ, Hao QL, Bin F, Kang RN, Dou BJ. Influence of Ce/Zr ratio on the synergistic effect over $CuCe_{1-x}Zr_xO_y$/ZSM-5 catalysts for the self-sustained combustion of carbon monoxide. Combust Sci Technol 2017;189:1394–415.
[4] Guo XL, Li J, Zhou RX. Catalytic performance of manganese doped CuO–CeO_2 catalysts for selective oxidation of CO in hydrogen-rich gas. Fuel 2016;163:56–64.
[5] Schönbrod B, Mariño F, Baronetti G, Laborde M. Catalytic performance of a copper–promoted CeO_2 catalyst in the CO oxidation: Influence of the operating variables and kinetic study. Int J Hydrogen Energy 2009;34:4021–8.
[6] Lee FC, Lu YF, Chou FC, Cheng CF, Ho RM, Tsai DH. Mechanistic study of gas-phase controlled synthesis of copper oxide-based hybrid nanoparticle for CO oxidation. J Phys Chem C 2016;120:13638–48.
[7] Zheng YN, Li KZ, Wang H, Wang YH, Tian D, Wei YG, et al. Structure dependence and reaction mechanism of CO oxidation: A model study on macroporous CeO_2 and CeO_2-ZrO_2 catalysts. J Catal 2016;344:365–77.
[8] Martínez-Arias A, Hungría AB, Fernández-García M, Conesa JC, Munuera G. Interfacial redox processes under CO/O_2 in a nanoceria-supported copper oxide catalyst. J Phys Chem B 2004;108:17983–91.
[9] Jia AP, Hu GS, Meng L, Xie YL, Lu JQ, Luo MF. CO oxidation over CuO/$Ce_{1-x}Cu_xO_{2-\delta}$ and $Ce_{1-x}Cu_xO_{2-\delta}$ catalysts: Synergetic effects and kinetic study. J Catal 2012;289:199–209.
[10] Kang RN, Wei XL, Bin F, Wang ZB, Hao QL, Dou BJ. Reaction mechanism and kinetics of CO oxidation over a CuO/$Ce_{0.75}Zr_{0.25}O_{2-\delta}$ catalyst. Appl Catal A Gen 2018;565:46–58.
[11] Skoglundh M, Thormählen P, Fridell E, Hajbolouri F, Jobson E. Improved light-off performance by using transient gas compositions in the catalytic treatment of car exhausts. Chem Eng Sci 1999;54:4559–66.
[12] Arnby K, Törncrona A, Andersson B, Skoglundh M. Investigation of Pt/γ-Al_2O_3 catalysts with locally high Pt concentrations for oxidation of CO at low temperatures. J Catal 2004;221:252–61.
[13] Bin F, Kang RN, Wei XL, Hao QL, Dou BJ. Self-sustained combustion of carbon monoxide over $CuCe_{0.75}Zr_{0.25}O_{\delta}$ catalyst: Stability operation and reaction mechanism. Proc Combust Inst 2019;37:5507–15.
[14] Arnby K, Assiks J, Carlsson P, Palmqvist A, Skoglundh M. The effect of platinum distribution in monolithic catalysts on the oxidation of CO and hydrocarbons. J Catal 2005;233:176–85.
[15] Wang C, Yua F, Zhua MY, Wang XG, Dan JM, Zhang JL, et al. Microspherical MnO_2-CeO_2-Al_2O_3 mixed oxide for monolithic honeycomb catalyst and application in selective catalytic reduction of NO_x with NH_3 at 50–150 °C. Chem Eng J 2018;346:182–92.
[16] Iojoiu EE, Bassou B, Guilhaume N. High-throughput approach to the catalytic combustion of diesel soot. Catal Today 2008;137:103–9.
[17] Frank-Kamenetskii DA. Diffusion and heat transfer in chemical kinetics. 2nd ed. New York: Plenum Press; 1969.
[18] Mccabe WL, Smith JC, Harriott Peter. Chem Eng Unit Oper 1993;4:527–65.
[19] Bin F, Wei XL, Li B, Hui KS. Self-sustained combustion of carbon monoxide promoted by the Cu-Ce/ZSM-5 catalyst in $CO/O_2/N_2$ atmosphere. Appl Catal B Environ 2015;162:282–8.
[20] Thormählen P, Skoglundh M, Fridell E, Andersson B. Low-temperature CO oxidation over platinum and cobalt oxide catalysts. J Catal 1999;188:300–10.
[21] Hornés A, Bera P, Cámara AL, Gamarra D, Munuera G, Arias AM. J Catal 2009;268:367–75.
[22] Qi L, Yu Q, Dai Y, Tang CJ, Liu LJ, Zhang HL, et al. Influence of cerium precursors on the structure and reducibility of mesoporous CuO-CeO_2 catalysts for CO oxidation. Appl Catal B: Environ 2012;119–120:308–20.
[23] Yao SY, Mudiyanselage K, Xu WQ, Johnston-Peck AC, Hanson JC, Wu TP, et al. Unraveling the dynamic nature of a CuO/CeO_2 catalyst for CO oxidation in operando: A combined study of XANES (Fluorescence) and DRIFTS. ACS Catal 2014;4:1650–61.
[24] Hornés A, Bera P, Cámara AL, Gamarra D, Munuera G, Arias AM. CO-TPR-DRIFTS-MS in situ study of CuO/$Ce_{1-x}Tb_xO_{2-y}$ (x = 0, 0.2 and 0.5) catalysts: Support effects on redox properties and CO oxidation catalysis. J Catal 2009;268:367–75.